

# Experimental Study on Coal Partial Gasification Coproducing Char, Tar, and Gas

SONG Xue, WANG Qinhu<sup>\*</sup>, ZHU Yao, XIE Guilin, ZHU Deao, CEN Jianmeng, LUO Zhongyang

State Key Laboratory of Clean Energy Utilization, Zhejiang University, Hangzhou 310027, China

© Science Press, Institute of Engineering Thermophysics, CAS and Springer-Verlag GmbH Germany, part of Springer Nature 2023

**Abstract:** The coal partial gasification process produces a large number of chars. They have similar combustion characteristics to anthracite and can be utilized as a material manufacturing clean briquette to replace residential coal to achieve clean combustion. Moreover, the coal partial gasification produced more tar at relatively low temperature, which can be applied as naphtha or diesel after purification and hydrogenation. Herein, experiments of coal partial gasification coproducing char, tar, and gas are carried out on a bench-scale fluidized bed reactor during the temperature range of 625–762°C. The effect of equivalence ratio on the characteristics of coal partial gasification products is studied. The results show that the equivalence ratio increasing from 0.06 to 0.13 leads to a higher partial gasification temperature and lower char yield, and tar yield reaches a maximum value and the lower calorific value of gas reaches as high as 6.14 MJ/m<sup>3</sup>. When the gasification temperature is lower than 643°C, the increase in temperature promotes the generation of oxygen-containing functional groups and aromatic compounds in coal particles, and the microstructures of char become more disordered. The combustion stability of char is getting worse, whereas the pore structures in char become abundant at high temperatures. From the analysis of the tar chromatography column, it is observed that asphaltene and non-hydrocarbon account for 77%–88% of the total amount of tar.

**Keywords:** coal partial gasification, cascading utilization, product characteristics

## 1. Introduction

Coal, a fossil fuel extensively used for residential heating especially in rural regions, accounts for approximately 57% of China's primary energy structure in 2020 [1–3]. Combustion of residential coal is prone to emit SO<sub>x</sub>, NO<sub>x</sub>, and other pollutants, which have a significant impact on human health and degradation of local air quality [4]. Char has been recognized as a new material manufacturing clean briquette to replace residential coal for achieving clean combustion in recent

years, attributed to its advantages of high calorific value, high fixed carbon, and low sulfur, etc. [5, 6]. In practical production, internal-heating semi-coke furnace is generally adopted to produce char through pyrolysis, especially in northern China [7, 8]. However, the major disadvantage of this process is scale-up issues, mainly due to the limited coal adaptability using lump coal as materials, and secondary pollution caused by the production of phenol-ammonia wastewater [9]. The staged coal conversion process has become one of the best ways to efficiency and comprehensive utilize

coal [10, 11]. And the coal staged conversion based on pyrolysis has been widely studied in char production [12, 13]. Meanwhile, since the coal pyrolysis process requires a large amount of external heat, the pyrolysis generally combines with another process that provides heat or heat carrier, resulting in high investment costs, complex systems, and difficult operation.

In recent years, coal partial gasification has attracted the attention of many researchers as a process to generate char tar gas within one reactor. Experiments and simulations involving coal staged conversion based on coal partial gasification aim to obtain syngas [14] or high hydrogen content gas [15] to produce hydrogen, SNG, etc., and char produced by gasification is sent to combustion furnace for power generation [14–16] and output for blast furnace injection [17]. The effect of gasified agent [18, 19], equivalence ratio [20], temperature [17], secondary air distribution modes [21] on partial gasification product characteristics has been explored by many researchers. However, most of those researches involving partial gasification are performed under higher gasification temperatures, ranging from 800°C to 1000°C, to prevent the tar formation. High reaction temperature contributes to a larger combustion share of char, in which the residual fixed carbon and volatile matter in char are less, and reaction activity is lower. Moreover, considering the necessary high reactivity of char for manufacturing clean briquette, studies on coal partial gasification at a relatively low temperature (less than 800°C) are in demand to clarify the composition and distribution of partial gasification products.

Based on this, the coal partial gasification coproducing char tar gas technology has been proposed by Zhejiang University. This process aims to produce char as the material making clean briquette and obtain tar production after purification. Meanwhile, adopting air as the

gasification agent has the advantages of higher energy, exergy efficiency, and lower equipment cost, which saves the expenditure of pure oxygen production in air separation equipment [22]. In addition, there are more combustible components in char, which possess high reactivity, and the char can be applied to produce a clean fuel such as briquette. The simplified process flowsheet is shown in Fig. 1. In this process, coal particles are transported into a fluidized bed gasifier together with air for partial gasification coproducing char, tar, and gas. The range of partial gasification temperature is set below 800°C. Partial gasification temperature can be controlled by regulating the equivalence ratio. With increasing equivalence ratio, the oxidation share of coal keeps rising, releasing more heat to instigate a gradual increment in gasification temperature.

Furthermore, a relatively low gasification temperature would result in an inevitable formation of tar during the coal partial gasification. In practical commercial production, the physical methods that have more simple operation and lower maintenance costs compared with chemical methods like catalytic conversion, are generally employed to remove the tar remaining in syngas, such as electric trapping, cyclone separation, etc. [23, 24]. During the process of coal partial gasification coproducing char tar gas, the tar is collected after tar physical removal equipment for further utilization. Meanwhile, coal tar is a complex organic mixture, which has low thermal instability and high viscosity. Application of coal tar, such as tar hydrogenation to produce light flux fuel, fine chemicals extraction, deep processing of asphalt, is determined by tar components [25, 26]. Hence, understanding of tar composition and precipitation characteristics during the coal partial gasification process is essential for tar application. But up to now, the researches about the components of tar obtained by coal partial gasification and the influence of

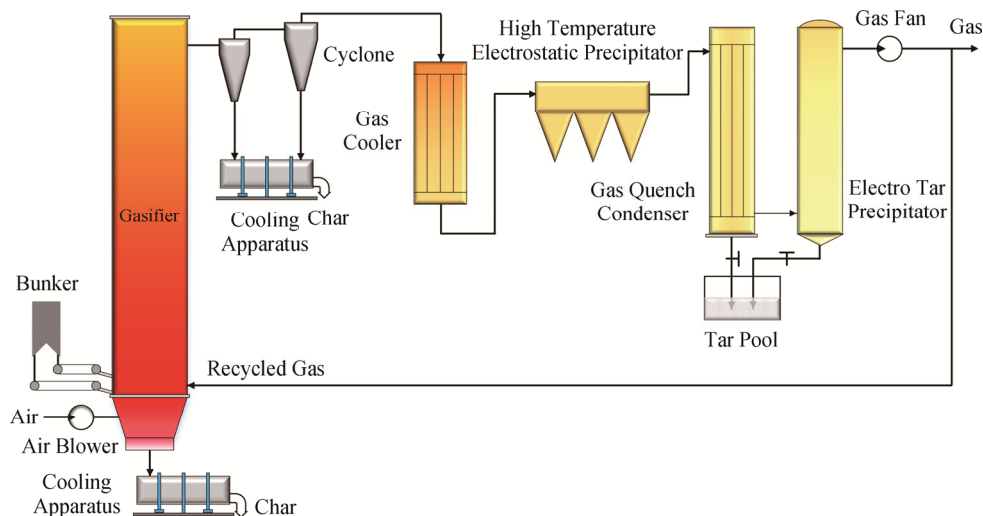


**Fig. 1** Flowsheet of coal partial gasification coproducing char gas tar in one fluidized bed reactor

reaction conditions on components of the tar are rarely seen. Therefore, a complete understanding of coal partial gasification characteristics under relatively low gasification temperature is necessary.

To sum up, researches on partial gasification in the existing literature are mainly carried out mainly at high temperatures (800°C–1000°C). There is a lack of experimental data on the characteristics of char and tar obtained from coal partial gasification at lower temperatures (below 800°C) in a fluidized bed reactor. Therefore, based on the coal partial gasification coproducing char tar gas technology proposed by Zhejiang University, the experiments of coal-air partial gasification were conducted in this paper. At the gasification temperature range from 625°C to 762°C, the effects of different equivalence ratios on the pore structure, carbon morphology, and combustion characteristics of char, and gas components were investigated. Furthermore, the composition and precipitation characteristics of tar were explored. This paper aims to study the distribution and characteristics of coal partial gasification products at the gasification temperature below 800°C, and to provide new data for the coal partial gasification with air in the commercial gasification system.

## 2. Experimental Section

### 2.1 Samples

The Gansu Huating coal adopted for the experiments was crushed into particles, and then sieved from 0.3 mm to 0.9 mm. The quartz sand employed as bed material in

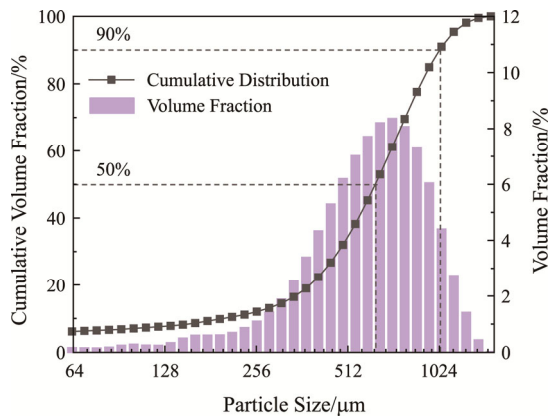


Fig. 2 Particle size distribution of pulverized coal

the experiments was sieved from 0.2 mm to 0.45 mm before use. The particle size distribution of pulverized coal is performed by a laser particle analyzer (Beckman Coulter LS13320), and the results are illustrated in Fig. 2. The particle size distribution of pulverized coal in the cumulative volume fractions of 50% and 90% was 0.63 mm and 1.03 mm, respectively. The raw coal and quartz sand were dried at 105°C for 6 h and sealed for storage before experiments. Moreover, the proximate and ultimate analysis of Gansu Huating coal is shown in Table 1. The proximate and ultimate analysis of coal was performed according to standard GB/T121-2008 [27] and GB/476-2015 [28], respectively.

### 2.2 Experimental facility

The coal partial gasification experiments were carried out in a bench-scale fluidized bed reactor. As shown in Fig. 3, the experimental system is mainly composed of fluidized bed reactor, gas feeding system, coal feeding system, gas-solid separation system and DCS system. The inner diameter of the lower part and higher part of the furnace was 80 mm and 120 mm, respectively, and the height of furnace was 2600 mm. The furnace was made of ceramics, and four groups of electric heating wires (1#, 2#, 3#, and 4#) around the furnace were used to preheat the furnace and reduce partial thermal dissipation. Meanwhile, in order to enhance the heat preservation capacity of the furnace, the furnace was surrounded by insulation cotton and insulation cement, and the outermost was a steel shell. The air was input by a centrifugal fan, and then heated to 200°C by two preheaters before entering the furnace. The pulverized coal was fed by a screw feeder. The speed of the screw feeders was controlled by the DCS system. The tar was captured by three serpentine quartz tubes and the filters in the tar trap were cooled by an ethanol cryogenic bath (−40°C). The purified gas samples were then collected by gas bags.

### 2.3 Partial gasification experiments

The coal partial gasification experiments were carried out in the following steps: (1) Turn on the heating weir of the preheaters and furnace; set the temperature of the preheater and furnace to 200°C and 600°C, respectively; open the ethanol cryogenic bath; set the constant temperature at −40°C. (2) Turn on the centrifugal fan to induce air into the furnace to ensure that the bed material

Table 1 Proximate and ultimate analysis of Gansu Huating coal

Proximate analysis/wt% (ad)				Ultimate analysis/wt% (ad)					$Q_{\text{net,ad}}$ /MJ·kg <sup>-1</sup>
M	A	V	FC	C	H	N	S	O*	
3.54	22.85	26.35	47.26	59.09	2.7	0.73	0.51	10.52	21.85

Note: ad: as air dried basis. \*: by subtraction

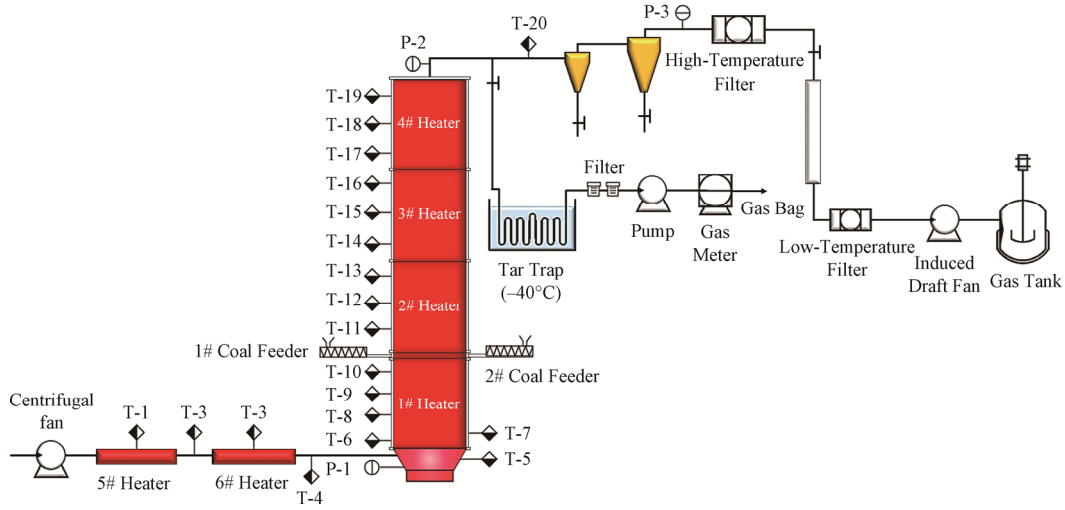


Fig. 3 Schematic diagram of the experimental system

flows. (3) Add 1000 mL (approximately 1.3 kg) of quartz sand to the furnace, and add about 3 kg of coal to the screw feeder. (4) Open the screw feeder, add the coal into furnace, and adjust the air-coal ratio to a required gasification temperature in the range of 600°C to 800°C. Meanwhile, set the temperature of heating weir to the average temperature of the furnace. (5) After the partial gasification was in a steady condition, the tar-sampling pipeline was opened and the purified gas sample was collected at a 15-minute interval, the results of gas components were averaged. The chars in the gasifier were collected by a char collection container cooled by N<sub>2</sub>. After 10-minute stabilized operation, char was discharged into the char collection container every two-minute interval, and each discharge lasted for around five seconds. (6) After 35 minutes, the coal feeder and the heating weir were stopped. Release air into the furnace for cooling.

The gas sample was collected from the top of the gasifier, and gas composition was analyzed by gas chromatography (GC, Agilent 7890BGC). Char and ash were collected from the bottom of the gasifier and two staged cyclones, respectively. The proximate and ultimate analysis of char were performed as same as coal. The pore structures of char samples were performed by the Brunauer-Emmitt-Teller (BET) analysis using a specific surface area and mesoporous analyzer (TriStar II). The carbon microstructures and crystalline structures of char samples were performed by a Raman spectroscopy (DXR Smart Raman). The char combustion characteristics were measured by a thermogravimetric analyzer (Thermax 500). The tar samples were separated by column chromatography analysis according to SY/T 5119-2008. First, the tar sample was separated into a hexane soluble fraction and asphaltene by hexane eluent. Then, the hexane soluble fraction of tar was separated into three fractions by silicone-Al<sub>2</sub>O<sub>3</sub> column

chromatography using hexane, dichloromethane/hexane, and anhydrous ethanol eluent. Therefore, the tar samples were isolated to asphaltene, saturated hydrocarbon, aromatic hydrocarbon and non-hydrocarbon, and the mass ratio of four components of tar was obtained.

The equivalence ratio (ER), defined as a ratio of air to coal in experimental condition divided by air to coal in stoichiometric condition, was calculated as Eq. (1).

$$ER = \frac{(\text{air/coal})_{\text{exp}}}{(\text{air/coal})_{\text{stoic}}} \quad (1)$$

Considering N<sub>2</sub> in gas, produced from coal partial gasification, was statistically inconsequential compared to the N<sub>2</sub> flow rate in the gasification agent, hence the gas volume could be calculated using the N<sub>2</sub> tracing method [11]. Therefore, the volume flowrate of syngas was calculated as Eq. (2).

$$V_{\text{gas}} = 100V_{N_2} / X_{N_2} \quad (2)$$

where  $V_{\text{gas}}$  (m<sup>3</sup>/h) represents the volume of gasification gas;  $X_{N_2}$  (%) represents the volume fraction of N<sub>2</sub> in the syngas.

The coal conversion, from coal to syngas, was calculated as Eq. (3).

$$\alpha_C = 100 \times (12V_{\text{gas}} \sum X_n / 22.4) / (M_{\text{coal}} \times C_{\text{ad}}) \quad (3)$$

where  $\alpha_C$  (%) represents coal conversion;  $X_n$  (%) represents the volume fraction of CO, CO<sub>2</sub>, CH<sub>4</sub>, C<sub>2</sub>H<sub>4</sub>, C<sub>2</sub>H<sub>6</sub>, C<sub>3</sub>H<sub>6</sub>, and C<sub>3</sub>H<sub>8</sub> in the syngas;  $M_{\text{coal}}$  (kg/h) represents the mass of coal feed;  $C_{\text{ad}}$  (%) represents the carbon content in raw coal.

According to the principle of the ash balance, the conversion ratios of carbon of coal,  $\alpha_{CA}$ , during the coal partial gasification was calculated as Eq. (4).

$$\alpha_{CA} = 100 \times [1 - (A_{\text{ad}} \times C_{\text{char,ad}}) / (A_{\text{char,ad}} \times C_{\text{ad}})] \quad (4)$$

where  $\alpha_{CA}$  (%) represents the carbon conversion of coal calculated by ash balance.  $A_{\text{ad}}$  (%) and  $A_{\text{char,ad}}$  (%)

represent the ash content in raw coal and char, respectively.  $C_{\text{char,ad}}$  (%) represents the carbon content in char.

The lower heating value of syngas was calculated as Eq. (5).

$$LH_{\text{gas}} = \sum V_i LH_i \quad (5)$$

where  $LH_{\text{gas}}$  ( $\text{MJ}/\text{m}^3$ ) represents the lower calorific value of syngas;  $V_i$  represents the volume fraction of various combustible components in syngas, including  $\text{CO}$ ,  $\text{CH}_4$ ,  $\text{C}_2\text{H}_4$ ,  $\text{C}_2\text{H}_6$ ,  $\text{C}_3\text{H}_6$ ,  $\text{C}_3\text{H}_8$ ,  $LH_i$  ( $\text{MJ}/\text{m}^3$ ) represents the lower calorific value of various combustible components.

The yields of char and tar produced by coal partial gasification were calculated as Eqs. (6) and (7).

$$Y_{\text{char}} = M_{\text{char}}/M_{\text{coal}} \times 100 \quad (6)$$

$$Y_{\text{tar}} = M_{\text{tar}}/M_{\text{coal}} \times 100 \quad (7)$$

where  $Y_{\text{char}}$  (%) and  $Y_{\text{tar}}$  (%) represent char and tar yield, respectively;  $M_{\text{char}}$  (kg/h) and  $M_{\text{tar}}$  (kg/h) represent the mass of char and tar.

In the commercial coal gasification plant, the gasification temperature is adjusted by changing the supplied coal or gasification agent to regulate the gasification reaction process. The experimental conditions are summarized in Table 2. The coal feed was kept at 2.61 kg/h, and the air volume flow was adjusted to carry out the variety of equivalence ratios. The value of the equivalence ratio ranged from 0.06 to 0.13. In this paper, the partial gasification temperature was represented by the T-9, which was inserted into the dense phase zone of the gasifier (see Fig. 3).

**Table 2** Experimental conditions

Experimental condition	1	2	3	4	5
Coal loading/ $\text{kg}\cdot\text{h}^{-1}$	2.61	2.61	2.61	2.61	2.61
Equivalence ratio*	0.06	0.08	0.10	0.11	0.13
Temperature/ $^{\circ}\text{C}$	625	643	695	736	762

Note: \* retain two decimals.

### 3. Results and Discussion

#### 3.1 Product yield analysis

The change in the volume fraction of gas composition with equivalence ratio is presented in Fig. 4. The total volume fraction of  $\text{H}_2$ ,  $\text{CO}$ , and  $\text{C}_2\text{-C}_3$  in gasification gas accounted for approximately 20%. As the equivalence ratio increased, the oxidation share of coal kept rising, which could release more heat to instigate increment of gasification temperature. The content of  $\text{CH}_4$  showed a slightly downward trend, which stemmed from more  $\text{CH}_4$  decomposing under high temperatures. When the equivalence ratio increased from 0.06 to 0.11, the content of  $\text{H}_2$  and  $\text{CO}$  increased by 2.10% and 2.85%, respectively, while that of  $\text{CO}_2$  decreased. This indicated that the higher the air concentration is, the more the released heat by the

coal combustion reaction is, which makes the Boundouard reaction and water gas reaction be enhanced, resulting in more  $\text{CO}$  and  $\text{H}_2$  and less  $\text{CO}_2$  production. The  $\text{H}_2$  content decreased slightly when equivalence ratio was further increased, which could attribute to  $\text{H}_2$  combustion.

Furthermore, the coal feeding rate in the experiment was constant (see Table 2). As the equivalence ratio increased, more  $\text{N}_2$  would enter into the furnace with air. And the more coal combusted, the more  $\text{CO}_2$  was generated. However, it can be seen from Fig. 4 that the proportion of  $\text{N}_2$  and  $\text{CO}_2$  in gas did not show an increasing trend as the equivalence ratio kept rising, which was different from the conclusion in the literature [29]. Thus, the variation in the yield of gas components with equivalence ratio is shown in Fig. 5. The yield of  $\text{CO}_2$  is higher than that of other gas components and increases with increasing temperature. The high oxygen content in Gansu Huating coal (10.52%) leads to the pyrolysis of coal particles under the condition of low equivalence ratio to generate more  $\text{CO}_2$ . With the increase of equivalence ratio, the  $\text{CO}_2$  yield increases continuously, owing to increasing combustion share of coal particle and combustible gas. With the equivalence ratio improving from 0.06 to 0.10, there was a small

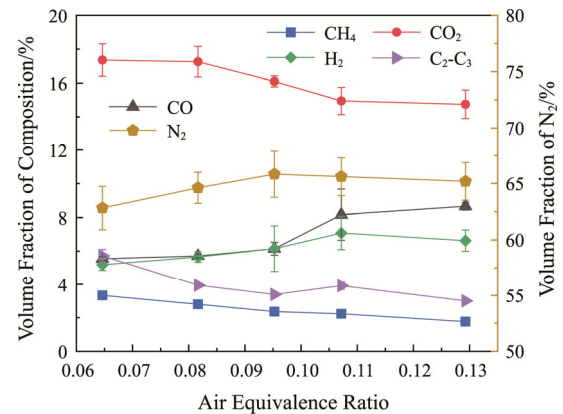


**Fig. 4** Effects of the equivalence ratio on the gas composition

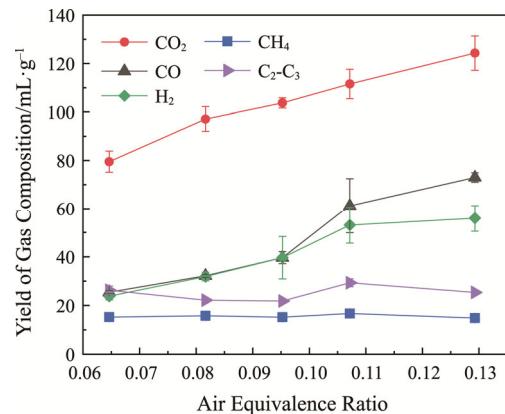


**Fig. 5** Effects of equivalence ratio on the yields of gas compositions

amount of  $C_2$ - $C_3$  decomposed in syngas. However, when the equivalence ratio further enhanced, the tar and straight chain hydrocarbons generated by gasification would undergo secondary cracking to generate  $C_2H_6$ ,  $C_3H_6$ , and  $C_3H_8$ . Furthermore, the aliphatic side chains of aromatic and aliphatic hydrocarbons would be decomposed into  $C_2$  at temperature around  $700^\circ C$  [30], resulting in a slight increase in  $C_2$ - $C_3$  at the later stage of the reaction. Intuitively speaking, the yield of the gas compositions continuously increased with increasing equivalence ratio.

The effect of equivalence ratio on the gasification temperature, coal conversion, carbon conversion, and lower calorific value of gas is shown in Fig. 6. The results showed that the gasification temperature kept a rise from  $625^\circ C$  to  $762^\circ C$  as the equivalence ratio increased. This could be ascribed to the combustion of more coal and combustible gas, which released more heat to raise the system temperature. It can be seen that both  $\alpha_{CA}$  and  $\alpha_C$  were generally on the rise as the equivalence ratio increased, indicating that higher equivalence ratio facilitated the burn-out of carbon in coal particle. The coal conversion rate improved by 43.68% with the equivalence ratio increasing from 0.06 to 0.11, which was more noteworthy than that (10.93%) as the equivalence ratio increased from 0.11 to 0.13. This result is consistent with the conclusion in the literature that the reaction rate first increased and then gradually decreased during the partial gasification process [31, 32].

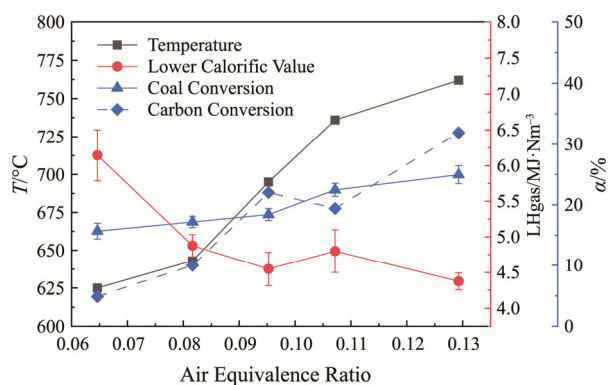


**Fig. 6** Effects of equivalence ratio on gasification temperature, lower calorific value of gas, coal conversion, and carbon conversion

Since the gasification agent adopted in this experiment was air, a large amount of nitrogen entered the furnace while the air supply is increased. Hence, as the equivalence ratio increases, the calorific value of syngas tends to decrease. The coal partial gasification at lower temperatures was supplied with less air, which resulted in a higher share of pyrolysis of coal. Thus, higher calorific value gas could be obtained when it was compared with high temperature partial gasification. When the equivalence ratio was 0.06, the low calorific value of coal

gas in this experiment reached the highest value, which was  $6.14 MJ/m^3$ . At higher temperature ( $736^\circ C$ ), the calorific value of the syngas exhibited a slight increment since the combustible gas produced by the combustion of the volatile precipitates in the coal was combusted. Therefore, it can be concluded that as the temperature increasing, the calorific value of syngas produced by coal air gasification jointly depends on the removal efficiency of volatiles in coal, the combustion of combustible gas and the amount of nitrogen entering the furnace.

The yields of char and tar obtained from coal partial gasification with different equivalence ratios are illustrated in Fig. 7. The char yield decreased continuously from 74.82% to 52.40% with the increase of the equivalence ratio. Due to the increasing equivalence ratio, more coal particles reacted with  $O_2$ , resulting in a decrement in the char yield. Furthermore, as the equivalence ratio increased from 0.06 to 0.11, the tar yield increased from 4.00% to 8.38%. It indicated that at low temperature (less than  $736^\circ C$ ), the exothermic reactions were strengthened with an increasing equivalence ratio; thus more volatile matter was removed from the coal particles, and the reaction of coal decomposing to organic matter was enhanced. However, with a further increment of air supply, the tar yield decreased from 8.38% to 5.65% as the temperature increased, indicating that increasing equivalence ratio promoted the secondary cracking and oxidation of the tar. It also expressed in the literature that the more  $O_2$  existence led to the increase of gasification temperature, which promoting the tar secondary decomposition [19, 33].

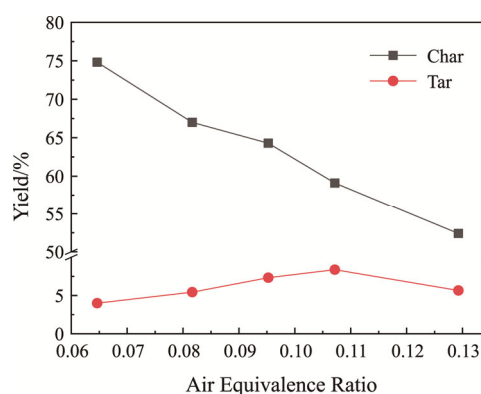


**Fig. 7** Char and tar yields of coal partial gasification at different equivalence ratios

### 3.2 Char characterization

To obtain char characteristics under five kinds of experimental conditions listed in Table 2, the BET analysis and Raman spectroscopy analysis of the pulverized coal and chars were adopted. Furthermore, the combustion behavior of the chars was measured through the thermo-gravimetric analyzer. Char samples under five

experimental conditions shown in Table 2, from low temperature to high temperature, were labeled as char-1, char-2, char-3, char-4, and char-5 in the following parts.

### 3.2.1 Pore structures of char samples

BET analysis is normally used to obtain the pore and surface features of chars. Fig. 8 shows the  $N_2$  adsorption/desorption isotherms of char samples obtained from the experiments under three gasification temperatures, 625°C, 695°C, and 762°C. According to the classification of the adsorption behavior of porous materials, the adsorption isotherms of the char samples were basically analogous to the combination of type I and type II adsorption curves. As visible in Fig. 8, with increasing gasification temperature, the adsorption capacity of char strengthened gradually, suggesting that the char had a more abundant pore structure as the gasification temperature increased. Simultaneously, the hysteresis phenomenon in nitrogen adsorption isotherms is usually associated with capillary condensation in mesopore structures. Moreover, the adsorption and desorption curves of the char under different pressures were close to the parallel state, which belonged to the type-H4 hysteresis loop. It indicated that the pore structures of char samples collected from the gasification experiments could be composed of one end closed blind pores, parallel plate gap pores, narrow crack pores, and ink bottle pores [34].

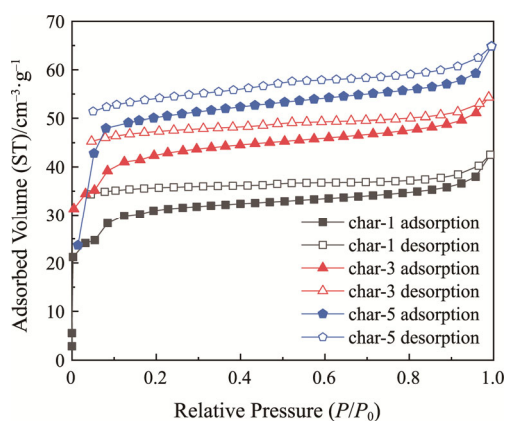


**Fig. 8** Adsorption/desorption isotherms of char at different conditions

The results of the BET specific surface and pore structure characteristics of five kinds of char at different temperatures are listed in Table 3. There was a larger BET specific surface area ( $S_{BET}$ ) and pore volume ( $V_{total}$ ) of char under the higher experiment temperature. It indicated that with increasing temperature,  $O_2$  molecules entered the inner surface of char particles through pores generated by the gasification reaction, which motivated the rapid removal of volatile matter and moisture, and more chars participated in the gasification. With the further gasification reaction of chars, more pores were

generated in the char particles, resulting in an increase in the total specific surface area ( $S_{BET}$ ) of the char samples [31, 35]. Moreover, with an increment in the specific surface area, more  $O_2$  entered into the char, and the degree of gasification reaction was deepened, thus improving the carbon conversion rate of the coal, which is consistent with the results displayed in Fig. 6. Since there are  $O_2$  active sites on the surface of the coal particles [36], more coal particles reacted with  $O_2$ , and the concentration of  $O_2$  active sites on the surface of the char particles gradually decreased. When the air flow entering furnace increased, the  $O_2$  concentration in the furnace increased, and the flammable components in the gas began to react with  $O_2$ , resulting in a decrease in the  $H_2$  content (see Fig. 4).

### 3.2.2 Raman spectra acquisition of char

Raman spectroscopy can be catholically used to analyze the microstructure features of carbonaceous material, and the Raman diffraction is generated by the rotation and vibration of molecules to change their polarizability [37]. In the Raman spectra, the carbon morphology in carbonaceous materials is often represented by graphite structure (G) and disordered structure (D) [38]. Owing to the overlap of G and D bands, the Raman spectrum, ranging from  $800\text{ cm}^{-1}$  to  $2200\text{ cm}^{-1}$  (covering the first-order Raman spectra), is subject to deconvoluting into four Lorentz bands ( $D_1$ ,  $D_2$ ,  $D_4$ , and G) and one Gaussian band ( $D_3$ ) by peak fitting [37, 39]. The deconvoluted Raman spectrum of Gansu Huating coal is displayed in Fig. 9. The  $1580\text{ cm}^{-1}$  band

**Table 3** Specific surface area and pore structure characteristics of char

Samples	$S_{BET}/\text{m}^2\cdot\text{g}^{-1}$	$S_{mic}/\text{m}^2\cdot\text{g}^{-1}$	$V_{total}/\text{cm}^3\cdot\text{g}^{-1}$	$V_{mic}/\text{cm}^3\cdot\text{g}^{-1}$
Char-1	101.733	65.328	0.065	0.032
Char-2	134.055	91.855	0.081	0.045
Char-3	137.899	91.318	0.079	0.045
Char-4	153.301	107.870	0.092	0.052
Char-5	162.693	127.886	0.099	0.062

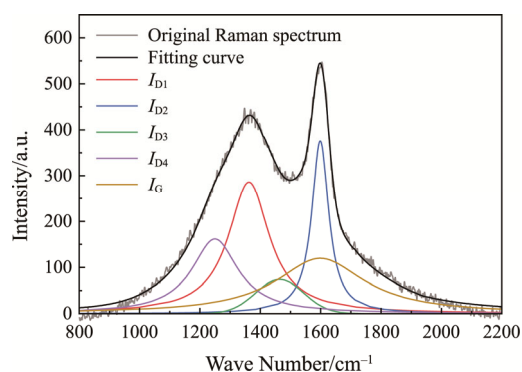


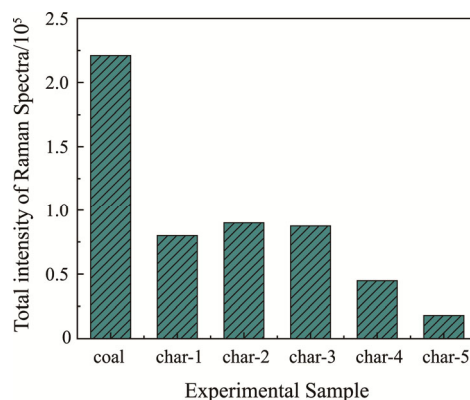
**Fig. 9** The deconvoluted Raman spectrum of Gansu Huating coal

**Table 4** Raman spectrum parameters of the coal and chars

Parameters	Coal	Char-1	Char-2	Char-3	Char-4	Char-5
$I_{D1}$	68 015.65	25 385.82	19 350.78	18 060.77	9 029.41	1 276.33
$I_{D2}$	38 838.12	5 248.34	14 481.52	6 060.75	2 146.14	2 516.48
$I_{D3}$	14 663.67	21 351.95	19 150.57	34 898.99	19 440.81	11 682.25
$I_{D4}$	42 984.8	10 465.61	7 959.28	4 050.77	1 478.37	231.47
$I_G$	56 495.2	17 476.88	28 991.95	24 368.90	12 799.39	2 220.98

(G band) is attributed to stretching vibration of the C=C bond in aromatic layers. The  $1350\text{ cm}^{-1}$  band ( $D_1$  band) is related to the aromatic ring which is more than six aromatic compounds or the disordered graphite lattice [40]. The  $1620\text{ cm}^{-1}$  band ( $D_2$  band) is considered as amorphous carbon with  $sp^2$  bond and involves the lattice vibration of the graphene layer [41]. The  $1530\text{ cm}^{-1}$  band ( $D_3$  band) represents the aromatic compounds containing less than six aromatic rings [42]. The  $1150\text{ cm}^{-1}$  band ( $D_4$  band) is considered as the stretching vibration of the  $sp^2$ - $sp^3$  bond of the crystallites or C-C and C=C in the conjugated polyene structure [40].

The integrated area of each band is typically used as a measurement to describe the corresponding Raman intensity [18, 43]. And the integrated area of each band ( $D_1$ ,  $D_2$ ,  $D_3$ ,  $D_4$ , and G) of the coal and chars is listed in Table 4. The high disorder degree of carbonaceous material gives rise to the large total Raman intensity. The electron-rich structures such as oxygen-containing functional groups are generally related to high Raman scattering ability. Therefore, the formation of aromatic rings or the consumption of oxygen-containing functional groups in the reaction process will lead to the decrement of the total peak area [44]. The total Raman peak area of Huating coal and chars under different gasification conditions are displayed in Fig. 10. The total peak intensity of coal was significantly higher than that of chars. This result was due to the coal containing more different alkyl side chains and functional groups, which make the structures of coal more disordered than that of the chars. Furthermore, Ye et al. investigate the characteristics of  $H_2O$ - $O_2$  coal partial gasification, and the results indicate that the char gradually becomes more disordered as the gasification temperature increases, which is due to the more drastic gasification reactions [18]. However, the total peak intensity of the char increased slightly with the increase in temperature (below  $643^\circ\text{C}$ ), indicating that the char structures became less ordered during this gasification stage. As the temperature improved further, the total peak intensity of the char gradually decreased, and the total peak intensity of the char sample at  $643^\circ\text{C}$  was larger than that of the other four char samples. It drew a conclusion different from the results of Ye et al. [18] and Tokmurzin et al. [17]. This difference could be explained by the fact that

**Fig. 10** Total intensity of Raman spectra of coal and chars

more oxygen-containing functional groups or aromatic compounds generated in coal particles as the temperature increased at the lower gasification temperature (less than  $643^\circ\text{C}$ ).

The ratios of the integrated area of some bands are used in general as indicators of the carbon structures in carbonaceous material [41].  $I_{D3}/I_{D1}$  is used instead as a parameter to characterize the ratio of small aromatic rings (aromatic rings less than six) to large aromatic rings.  $I_{D1}/I_G$  is employed instead as a parameter to characterize the disorder degree of the char [42, 45]. As shown in Fig. 11(a), there was a general trend that  $I_{D3}/I_{D1}$  increased with increasing gasification temperature. The observed increasing relative content of small to large aromatic rings in char order with increasing reaction temperature was consistent with those in the literature. Those in literature are increasing temperature (below  $900^\circ\text{C}$ ) would lead to the consumption of small aromatic rings or the transformation into large aromatic rings [18, 44, 46]. Furthermore, when comparing the  $I_{D1}/I_G$  of the chars obtained from different gasification temperatures, it was observed the overall trend of the decrement in  $I_{D1}/I_G$  with the increasing temperature, as seen in Fig. 11(b). It indicated that the char structures became less disordered and the reaction activity decreased with an increment of gasification temperature. The result herein also clarified the basis of coal partial gasification. During the gasification proceeding, the reactive parts of coal particles were increasingly consumed, and the higher carbon conversion rate required harsher reaction conditions.

### 3.2.3 Combustion characteristics

The non-isothermal combustion experiments were carried out to investigate the influence of reaction condition on the combustion characteristics of the char samples obtained from different gasification temperatures. The TG (thermogravimetry) curves and DTG (digital thermogravimetry) curves of chars are illustrated in Fig. 12(a) and Fig. 12(b), respectively. Fig. 12(c) shows the combustion characteristic temperature and maximum combustion rate ( $dw/dt$ )<sub>max</sub> of char-1 determined by the TG-DTG method [47]. Accordingly, the variation of maximum combustion rate and char combustion characteristic temperature is presented in Fig. 12(d) and Fig. 12(e), respectively. The ignition temperature ( $T_i$ ) of

char was generally on the rise as the gasification temperature increased. The results herein could be ascribed to the removal of residual volatile matter and combustion of fixed carbon in the char with increasing partial gasification temperature, which are consistent with the proximate and ultimate analysis results of the chars presented in Table 5. It resulted in a higher  $T_i$  of the char collected from the experiment under a higher gasification temperature, and combustion performance decreased appreciably. As seen in Fig. 12(d) and Fig. 12(e), when the gasification temperature increased from 625°C to 762°C, the temperature corresponding to the maximum combustion rate ( $T_{max}$ ) generally increased from 515.83°C to 544.83°C, and the maximum

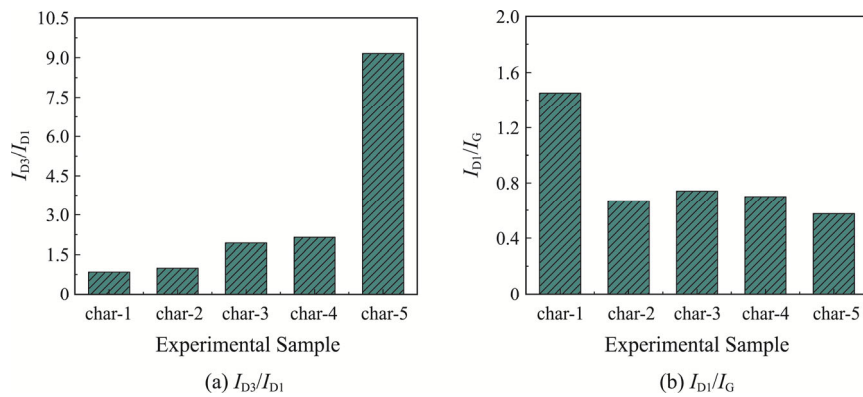


Fig. 11 Ratio of band peak areas of chars obtained from different conditions

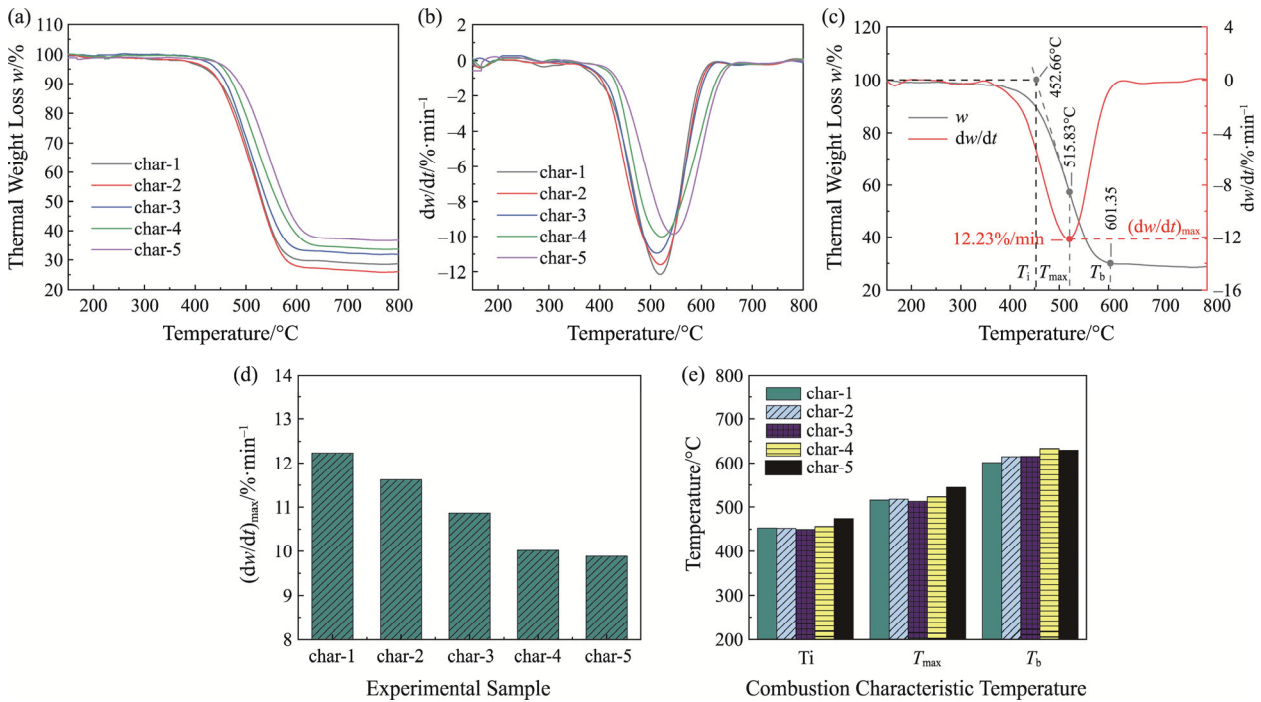


Fig. 12 Combustion characteristics of chars at different conditions. (a) TG curves of chars, (b) DTG curves of chars, (c) combustion characteristics of char-1, (d) the maximum combustion rate of chars, and (e) combustion characteristic temperature of chars obtained from different conditions

**Table 5** Proximate and ultimate analysis of char at different conditions

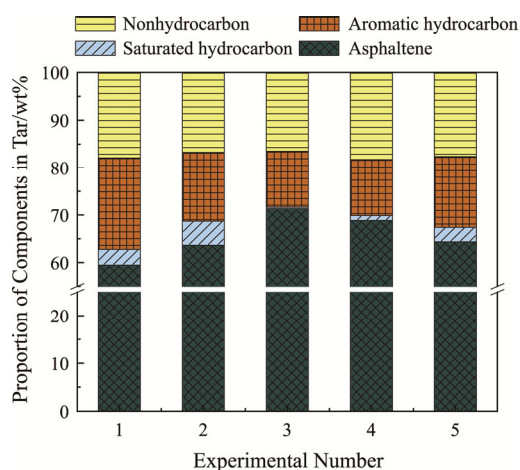
Samples	Proximate analysis/wt% (ad)				Ultimate analysis/wt% (ad)				
	M	A	V	FC	C	H	N	S	O*
Char-1	1.14	26.88	8.23	63.75	66.13	0.82	0.59	0.40	4.04
Char-2	1.13	28.06	7.20	63.15	65.31	0.71	0.63	0.37	3.79
Char-3	1.05	30.94	7.47	60.54	62.39	0.54	0.58	0.38	4.12
Char-4	1.04	30.75	5.51	62.70	64.09	0.31	0.58	0.36	2.87
Char-5	0.96	34.34	4.98	59.72	60.47	0.26	0.57	0.38	3.02

Note: ad: as air dried basis. \*: by subtraction

combustion rate decreased from 12.23%/min to 9.89%/min. Therefore, it can be concluded that there is a lower combustion rate and worse combustion stability of char obtained under a higher gasification temperature.

### 3.3 Tar characterization

In order to figure out the components of tar obtained from the coal partial gasification, the column chromatography separation results of tar were carried out. Tar samples with five gasification temperatures from low to high are labeled as tar-1, tar-2, tar-3, tar-4, and tar-5. The normalized results of proportion of non-hydrocarbon, aromatic hydrocarbon, saturated hydrocarbon and asphaltene in tar are illustrated in Fig. 13 to obtain the correlation between the reaction temperature and the components of tar. Among the four components of the tar, the highest and lowest content was asphaltene and saturated hydrocarbon, respectively. As the gasification temperature increased, the proportion of asphaltene in tar was found a continuous rise to a peak value of 71.33% at 695°C, and then gradually decreased. In contrast, the proportion of aromatic hydrocarbons continuously decreased to a minimum value, which was 11.84% at 695°C, and then increased slightly. These results can be explained by the enhancement of coal gasification reaction as temperature increased (higher than 695°C), resulting in the tar secondary creaking reactions that promoted the decrement of asphaltene proportion and the increment of light components content [48]. Furthermore, the gasification temperature marginally affected the proportion of saturated hydrocarbons, which accounted for 0.3%–6%. It was attributed to reactions between saturated hydrocarbons and O<sub>2</sub> at higher temperatures. It rapidly decomposed into polar groups and generated C<sub>x</sub>H<sub>y</sub>, H<sub>2</sub>, and CO<sub>x</sub>, and saturated hydrocarbons easily cracked and condensed to generate other components [30, 49]. Moreover, the temperature had little effect on the proportion of non-hydrocarbon in tar and its content was stable in the range of 16%–18%. In the case of the tar composition, non-hydrocarbons and asphaltene accounted for 77%–88%, which was higher than the proportion of non-hydrocarbons and asphaltene in the

**Fig. 13** Four components of tar at different conditions

low-medium temperature tar obtained from the typical coal pyrolysis [50]. However, non-hydrocarbons and asphaltene often contained a large number of polycyclic aromatic hydrocarbons, which resulted in the difficult transformation of tar by traditional fixed bed hydrogenation. Therefore, the suspension bed hydrogenation process with wide feedstock adaptability can be used to process the tar into clean fuel oil. Traditional distillation can also be employed to separate the tar into different distillates, and further extract a variety of chemical products [26, 51]. Coal tar pitch, which accounts for a high proportion of the tar, can be prepared building materials or synthetic materials through deep processing [25].

## 4. Conclusions

The coal partial gasification experiments at 625°C–762°C were carried out on a bench-scale fluidized bed gasifier. The equivalence ratios (0.06, 0.08, 0.10, 0.11, and 0.13) on (1) the yields of char, tar, and gas, (2) the pore structures, carbon morphology, and combustion characteristics of char, and (3) the composition and precipitation characteristics in tar were investigated. The following conclusions are drawn.

As the equivalence ratio increased from 0.06 to 0.13,

the gasification temperature kept rising from 625°C to 762°C, and the coal conversion and carbon generally increased, revealing that the higher equivalence ratio facilitated the burn-out of carbon in coal particle. The lower calorific value of gas produced by coal air gasification jointly depends on the efficiency of volatile matter removing from coal, the combustion of combustible gas and the entrance of nitrogen into furnace, which reached as high as 6.14 MJ/m<sup>3</sup>. While the char yield was gradually declined from 74.81% to 52.40%, the tar yield reached a maximum value of 8.38%, when the equivalence ratio was 0.11.

With increasing gasification temperature, the char structures became more disordered, resulting in higher reactivity due to the generation of oxygen-containing functional groups or aromatic compounds as the temperature was below 643°C. Then the char structures became more ordered in the late stage of the gasification. The pore structure of char became more abundant as the temperature increased from 625°C to 762°C, while the combustion stability worsened and the combustion performance decreased appreciably.

The asphaltene content of tar from coal partial gasification was the highest, accounting for 59%–71%, followed by the non-hydrocarbon and aromatic hydrocarbon. Saturated hydrocarbons accounted for the least, which was around 0.3%–6%. The tar obtained by coal partial gasification can be further processed by suspension bed hydrogenation or traditional jomdistillation to output as clean fuel oil or a variety of chemical products.

## Acknowledgments

This work is supported by the National Key Research and Development Projects of China (2019YFE0100100-05).

## Conflict of Interest

On behalf of all authors, the corresponding author states that there is no conflict of interest.

## References

- [1] BP, Statistical review of world energy - China's energy market in 2020, 2021-7-9. <https://www.bp.com/content/dam/bp/business-sites/en/global/corporate/pdfs/energy-economics/statistical-review/bp-stats-review-2021-china-insights.pdf>.
- [2] Zhou Y., Zi T., Lang J.L., et al., Impact of rural residential coal combustion on air pollution in Shandong, China. *Chemosphere*, 2020, 260: 1–9.
- [3] Krupal K., Mikuska P., Horak J., Hopan F., Kubonova L., Influence of boiler output and type on gaseous and particulate emissions from the combustion of coal for residential heating. *Chemosphere*, 2021, 278: 1–9.
- [4] Liang B., Bai H., Feng Q., Song H., Lan T., Liu X., Emissions of particulate matter and polycyclic aromatic hydrocarbons from household coal combustions. *CIESC Journal*, 2019, 70(8): 2888–2897.
- [5] Zheng S., Wang Z., Wang P., Cheng X., Xu H., Current status and progress of the clean and efficient utilization of pyrolysis semi-coke. *Huadian Technology*, 2020, 42(7): 42–49.
- [6] Yuan M., Wang C., Zhao L., Zhu Z., Wang P., Wang C., Che D., Evaluation and optimization of preparation for semi-coke briquette with alkali-heat treated wheat straw binder. *International Journal of Coal Preparation and Utilization*, 2020. DOI:10.1080/19392699.2020.1841176.
- [7] Ning X., Dang H., Zhang J., Wang G., Zhang N., Yue H., Research progress of low-order coal pyrolysis process and semi-coke production process. *Iron and Steel*, 2021, 56(1): 1–11.
- [8] Kang Y., Zou C., Zhao J., He J., Ma C., Zhang X., Microstructure characteristics of semi-coke under different pyrolysis processes and its influence on combustion performance. *Journal of Iron and Steel Research*, 2019, 31(7): 601–611.
- [9] Fang X., Analysis of quality improvement and utilization of internal-heating semi-coke furnace gas. *Coal Chemical Industry*, 2021, 49(5): 16–18, 38.
- [10] Gao J., Zhang Y., Meng D., Jiao T., Qin X., Bai G., Liang P., Effect of ash and dolomite on the migration of sulfur from coal pyrolysis volatiles. *Journal of Analytical and Applied Pyrolysis*, 2019, 140: 349–354.
- [11] Jia X., Wang Q., Cen K., Chen L., An experimental study of CaSO<sub>4</sub> decomposition during coal pyrolysis. *Fuel*, 2016, 163(1): 157–165.
- [12] Dai B.Q., Zhang L., Cui J.F., Hoadley A., Zhang L., Integration of pyrolysis and entrained-bed gasification for the production of chemicals from Victorian brown coal - Process simulation and exergy analysis. *Fuel Processing Technology*, 2017, 155: 21–31.
- [13] Jing X.Y., Zhu Z.P., Dong P.F., Meng G.J., Wang K., Lyu Q.G., Energy quality factor and exergy destruction processes analysis for a proposed polygeneration system coproducing semicoke, coal gas, tar and power. *Energy Conversion and Management*, 2017, 149: 52–60.
- [14] Ye C., Wang Q., Luo Z., Fang M., Cen K., Techno-economic analysis of novel power generation system based on coal partial gasification technology. *Asia-Pacific Journal of Chemical Engineering*, 2019, 14(6): e2377.
- [15] Ye C., Zheng Y.Q., Xu Y.S., Li G.N., Dong C., Tang Y.J., Wang Q.H., Energy and exergy analysis of

- poly-generation system of hydrogen and electricity via coal partial gasification. *Computers & Chemical Engineering*, 2020, 141(4): 106911.
- [16] Ye C., Ye Z.F., Zhu Z.J., Wang Q.H., Thermodynamic and economic analysis of oxy-fuel-integrated coal partial gasification combined cycle. *Acs Omega*, 2021, 6(6): 4262–4272.
- [17] Tokmurzin D., Adair D., Dyussekanov T., Suleymenov K., Golman B., Aiybetov B., Development of a circulating fluidized bed partial gasification process for co-production of metallurgical semi-coke and syngas and its integration with power plant for electricity production. *International Journal of Coal Preparation and Utilization*, 2019. DOI:10.1080/19392699.2019.1674842.
- [18] Ye C., Wang Q., Luo Z., Xie G., Jin K., Siyil M., Cen K., Characteristics of coal partial gasification on a circulating fluidized bed reactor. *Energy & Fuels*, 2017, 31(3): 2557–2564.
- [19] Ye C., Wang Q., Yu L., Luo Z., Cen K., Characteristics of coal partial gasification experiments on a circulating fluidized bed reactor under CO<sub>2</sub>-O<sub>2</sub> atmosphere. *Applied Thermal Engineering*, 2018, 130: 814–821.
- [20] Upadhyay D.S., Sakhiya A.K., Panchal K., Patel A.H., Patel R.N., Effect of equivalence ratio on the performance of the downdraft gasifier - An experimental and modelling approach. *Energy*, 2019, 168: 833–846.
- [21] Zhang Y., Zhu J., Lyu Q., Pan F., Experimental study on combustion characteristics of pulverized coal based on partial gasification of circulating fluidized bed. *Energy & Fuels*, 2020, 34(1): 989–995.
- [22] Ochnio M., Kluska J., Kardas D., Effects of biochar and ash outflow during updraft partial gasification on process parameters in a moving bed reactor. *Chemical Papers*, 2020, 74(11): 4047–4055.
- [23] Rios M.L.V., Gonzalez A.M., Lora E.E.S., del Olmo O.A. A., Reduction of tar generated during biomass gasification: A review. *Biomass & Bioenergy*, 2018, 108: 345–370.
- [24] Deng C., Song W., Chai Z., Guo S., Zhu Z., Characteristics of tar thermal cracking and catalytic conversion during circulating fluidized bed char gasification. *Energy & Fuels*, 2020, 34(1): 142–149.
- [25] Ma Z., Wei X., Liu G., Liu F., Zong Z., Value-added utilization of high-temperature coal tar: A review. *Fuel*, 2021, 292: 119954.
- [26] Xue H., Li H., Han X., Review on development status and prospect of comprehensive utilization of coal tar. *Modern Chemical Industry*, 2021, 41(S1): 105–109, 113.
- [27] GB/T 212-2008. Proximate analysis of coal. Beijing: Standards Press of China, 2008.
- [28] GB/T 31391-2015. Ultimate analysis of coal. Beijing: Standards Press of China, 2015.
- [29] Huang Y., Jin B., Zhong Z., Zhou H., Kong H., Experiment and research on partial coal gasification in circulated fluidized bed. *Coal Science and Technology*, 2003, 31(12): 20–22, 126.
- [30] Dun Q., Chen Z., Huang F., Zhou Y., Yu J., Gao S., Liu H., Influences of temperature and residence time on secondary reactions of volatiles from coal pyrolysis. *The Chinese Journal of Process Engineering*, 2018, 18(1): 140–147.
- [31] Ye C., Wang Q., Luo Z., Fang M., Cen K., Influence of reactant atmospheres and temperature on mechanism of gasification of coal char derived from lignite. *Energy Technology*, 2016, 4(6): 722–728.
- [32] Li Y., Zhang G., Yang Y., Zhai D., Zhang K., Xu G., Thermodynamic analysis of a coal-based polygeneration system with partial gasification. *Energy*, 2014, 72: 201–214.
- [33] Shamsi A., Catalytic and thermal cracking of coal-derived liquid in a fixed-bed reactor. *Industrial & Engineering Chemistry Research*, 1996, 35(4): 1251–1256.
- [34] Qi L., Tang X., Wang Z., Peng X., Pore characterization of different types of coal from coal and gas outburst disaster sites using low temperature nitrogen adsorption approach. *International Journal of Mining Science and Technology*, 2017, 27(2): 371–377.
- [35] Wang Q., Zhang R., Luo Z., Fang M., Cen K., Effects of pyrolysis atmosphere and temperature on coal char characteristics and gasification reactivity. *Energy Technology*, 2016, 4(4): 543–550.
- [36] Zhang R., Wang Q., Luo Z., Fang M., Cen K., Coal char gasification in the mixture of H<sub>2</sub>O, CO<sub>2</sub>, H<sub>2</sub>, and CO under pressured conditions. *Energy & Fuels*, 2014, 28(2): 832–839.
- [37] He X., Liu X., Nie B., Song D., FTIR and Raman spectroscopy characterization of functional groups in various rank coals. *Fuel*, 2017, 206: 555–563.
- [38] Sheng C., Char structure characterised by Raman spectroscopy and its correlations with combustion reactivity. *Fuel*, 2007, 86(15): 2316–2324.
- [39] Wang M., Roberts D.G., Kochanek M.A., Harris D.J., Chang L., Li C.Z., Raman spectroscopic investigations into links between intrinsic reactivity and char chemical structure. *Energy & Fuels*, 2014, 28(1): 285–290.
- [40] Azargohar R., Nanda S., Kozinski J.A., Dalai A.K., Sutarto R., Effects of temperature on the physicochemical characteristics of fast pyrolysis bio-chars derived from Canadian waste biomass. *Fuel*, 2014, 125: 90–100.
- [41] Wang B., Sun L., Su S., Xiang J., Hu S., Fei H., Char structural evolution during pyrolysis and its influence on combustion reactivity in air and oxy-fuel conditions. *Energy & Fuels*, 2012, 26: 1565–1574.
- [42] Tay H.L., Kajitani S., Zhang S., Li C.Z., Effects of

- gasifying agent on the evolution of char structure during the gasification of Victorian brown coal. *Fuel*, 2013, 103: 22–28.
- [43] Smith M.W., Dallmeyer I., Johnson T.J., Brauer C.S., McEwen J.S., Espinal J.F., Garcia-Perez M., Structural analysis of char by Raman spectroscopy: Improving band assignments through computational calculations from first principles. *Carbon*, 2016, 100: 678–692.
- [44] Li X., Hayashi J., Li C., FT-Raman spectroscopic study of the evolution of char structure during the pyrolysis of a Victorian brown coal. *Fuel*, 2006, 85(12–13): 1700–1707.
- [45] Knauer M., Carrara M., Rothe D., Niessner R., Ivleva N.P., Changes in structure and reactivity of soot during oxidation and gasification by oxygen, studied by micro-Raman spectroscopy and temperature programmed oxidation. *Aerosol Science and Technology*, 2009, 43(1): 1–8.
- [46] Zhang R., Liu D., Wang Q., Luo Z., Fang M., Cen K., Coal char gasification on a circulating fluidized bed for hydrogen generation: experiments and simulation. *Energy Technology*, 2015, 3(10): 1059–1067.
- [47] Muhetaer S., Wang Q., Tang J., Si W., Yu L., Luo Z., Experimental research on the influence of CO<sub>2</sub> on fluidized bed pyrolysis of bituminous coal. *Proceedings of the CSEE*, 2018, 38(13): 3881–3888.
- [48] Xu W.C., Tomita A., The effects of temperature and residence time on the secondary reactions of volatiles from coal pyrolysis. *Fuel Processing Technology*, 1989, 21(1): 25–37.
- [49] Wang G., Zhou A., Time evolution of coal structure during low temperature air oxidation. *International Journal of Mining Science and Technology*, 2012, 22(4): 509–513.
- [50] Shi Z., Fang M., Wang Q., Luo Z., Studies on rapid pyrolysis characteristics of Huainan coal. In: *International Conference on Energy Engineering and Environmental Engineering 2013*, Hangzhou, China. Switzerland: Trans Tech Publications Ltd, 2013, pp. 32–35.
- [51] Li C., Suzuki K., Resources, properties and utilization of tar. *Resources Conservation and Recycling*, 2010, 54(11): 905–915.